Research Article

Meng Gao*, Mengying Li, Jiahao Wang, Pengfei Yang, and Mengge Xu

Effect of fly ash on properties and hydration of calcium sulphoaluminate cement-based materials with high water content

https://doi.org/10.1515/rams-2024-0046 received August 03, 2023; accepted July 08, 2024

Abstract: In this study, the effects of fly ash (FA) on the setting time, compressive strength, and hydration evolution of calcium sulphoaluminate (CSA) cement-based materials with high water content were investigated, targeting the design of a modified high-water material to delay excessively rapid setting time and enhance later-age strength. This was investigated using a combination of X-ray diffraction (XRD), Fourier transform infrared resonance (FTIR) spectroscopy, and Thermogravimetric Analysis (TGA). The results showed that the setting time of the high-water materials was delayed by increasing the FA content, with 15% being the optimal dosage for the setting time. A 5-10% content of FA is conducive to the development of later-age compressive strength and has a slight adverse effect on the early-age compressive strength of high-water materials. The microscopic test results show that FA mainly acts as a microaggregate in the early-age hydration process, whereas in the later-age hydration process, it promotes gypsum consumption and C₂S hydration to form ettringite. The incorporation of FA effectively promotes ettringite formation in CSA cement-based materials with high water content. Therefore, the addition of FA can enhance the overall performance of high-water materials to a certain extent, and the long-term strength development of the material can satisfy engineering requirements.

Keywords: fly ash, calcium sulphoaluminate cement, highwater materials, hydration process, ettringite

1 Introduction

With the rapid development of economic, scientific, and technological activities, the scale of coal exploitation and utilisation as one of the primary energy sources is increasing worldwide [1-3]. Coal mining provides raw materials for metallurgical, chemical, iron, and steel industries but also causes several problems, such as waste of resources, surface damage caused by security risks, and environmental pollution. The environmental damage caused by coal mining in underground goafs can be effectively mitigated using backfill materials. However, backfilling materials are still mainly Portland cement, and there are drawbacks in the complex process and high cost [4,5]. The calcium sulphoaluminate (CSA) cement developed in China in 1970 is characterised by environmental protection, early strength and quick setting, and low drying shrinkage [6,7]. It is widely used in repair materials, low-temperature construction, precast concrete products, anti-seepage materials, and other construction fields [8-10], providing conditions for developing high-water materials.

High-water material is a new type of double-liquid backfill material with a high water-solid ratio of up to 1.5–3.0, and the volume water content in the system can reach 85-90%. High water materials include high aluminium, sulphur aluminium, and iron aluminium types. Sulphur-aluminium-based high-water materials are relatively affordable and widely used [11-14]. The sulphonatebased high-water material is composed of slurries A and B. Slurry A includes CSA cement, a suspension agent, a retarder, and a dispersant. Slurry B is composed of gypsum, lime, an accelerator, an early strength agent, and a suspension dispersant. Slurries A and B can stand for a prolonged period without setting before stirring, and rapid solidification and early strength are achieved after stirring [15]. The hydration reaction formulas of sulphonate-based high-water material are as follows [16,17] (using simplified naming, C = CaO, $S = SiO_2$, $A = Al_2O_3$, $\bar{S} =$ SO_3 , H = H_2O):

^{*} Corresponding author: Meng Gao, School of Civil Engineering, Henan University of Technology, Zhengzhou, 450001, China; Henan Key Laboratory of Grain and Oil Storage Facility & Safety, HAUT, Zhengzhou, 450001, China, e-mail: gaomeng88@haut.edu.cn Mengying Li, Jiahao Wang, Mengge Xu: School of Civil Engineering, Henan University of Technology, Zhengzhou, 450001, China Pengfei Yang: China Construction Seventh Engineering Bureau Co., LTD, Zhengzhou, 450001, China

2 — Meng Gao et al. DE GRUYTER

$$C_4A_3\bar{S} + 18H \rightarrow C_3A\bar{S}_3H_{12} + 2AH_3$$
, (1) admixtures [29,30]. Xiao [31,32] and Zhou *et al.* [33] showed $3C_4A_3S + 2C\bar{S}H_2 + 34H \rightarrow 3C_6A\bar{S}_3H_{32} + 4AH_3$, (2) that the dissolution rate of silica-aluminium solid waste with low content in the CSA system was slow but gradual, and the strength increase was delayed. CSA cement also effectively reduces the overall shrinkage of hardened slurry. This not only achieves the purpose of energy saving and carbon reduction but also improves the performance of CSA $C_4A_3\bar{S} + 8C\bar{S}H_2 + 6CH + 74H \rightarrow 3C_6A\bar{S}_3H_{32}$, (6) cement-based materials.

Fly ash (FA) is a typical silica-aluminium solid waste

The above reaction formulas show that in a high-water system, the CSA cement guickly reacts with anhydrite and lime and generates substantial acicular ettringite crystals, forming a dense microstructure. Gypsum is necessary for the formation of ettringite in the system, and lime accelerates ettringite formation during the hydration reaction. The role of C₄A₃S̄ in CSA cement is to rapidly convert a large amount of free water in the system into the ettringite crystal water, rapidly setting the mixed slurry [18]. The hydration of β-C₂S in cement produces calcium silicate hydrates. Once the high-water material is transported to the underground goaf, it rapidly solidifies and forms a backfill of a certain strength, thereby reducing the degree of damage caused by resource mining on the surface. Highwater materials have broad application prospects in mine engineering, tunnel support, gob backfill, oil well plugging, port engineering, and other fields [19-21].

The various components and curing conditions of highwater materials affect their performance and engineering applications. Xia et al. [22] indicated that high-water materials exhibited the optimal compressive strength and highest hydration heat release when the content of gypsum and lime is in the ranges of 80-85% and 20-15%. Regarding the external conditions, the water temperature and curing temperature mainly affect the early and late performance of high-water materials [23], and increasing the water-cement ratio prolongs the setting time of materials and reduces the compressive strength [24]. The rapid solidification of highwater materials leads to difficulties in pumping, late strength improvement, and high economic cost; therefore, optimisation of admixtures is the most used method [25-27]. Although lithium carbonate, slag, silica fume, and other auxiliary materials have been used to improve high-watercontent materials, they are generally scarce and expensive. In summary, the main reason for defects in high-water material is closely related to the performance of CSA cement [28]. The use of additional silica-aluminium solid waste to optimise the performance of CSA cement-based materials is more environmentally friendly and cheaper than chemical

Fly ash (FA) is a typical silica-aluminium solid waste material, which is commonly used as a precursor material to produce alkali-activated material (AAM) [34–37]. Abdulrahman *et al.* [38] and Qin *et al.* [39] used FA to improve the quality defects of recycled aggregate and limitations of brittle concrete materials in geopolymer recycled aggregate concrete. Xiao *et al.* [40] compared the reaction degree of coal gasification fly ash with OPC, CH, and alkali-binary systems, which increased sequentially and slowly with curing time. The cost of a CH-FA sample is much lower than that of an OPC-FA/alkali-excited sample. The main function of slurry B in high-water material is to provide a calcium source to generate CH. In addition, the strength of CSA cement mortar decreases with the increase of FA, and the reaction degree of FA in CSA cement is approximately 20–30% [41].

Some researchers have also studied the effects of FA on high-water materials. Li et al. [42] showed that FA with a higher calcium content exhibited the highest strength among high-water materials. Sun et al. [43,44] substituted 60% FA for the high-water material prepared using CSA cement, and the hydration heat release peak and cost were reduced by 22.9 and 54.6%, respectively. Although incorporating FA reduces the hydration rates and costs, excessive incorporation of FA results in excessive earlystrength reduction incompatible with engineering applications. Most existing studies on the application of FA in high-water materials focused on the properties of FA and improving the macroscopic properties of high-water materials. There is a lack of comprehensive analysis of the physicochemical properties and quantitative summary of the hydration mechanism of high-water materials after replacing CSA cement with low-content FA.

This study investigated the influence of FA content on the setting time and compressive strength of CSA cement-based high-water materials with a water-to-solid ratio of 3.0. The hydration products of the modified high-water materials were qualitatively and quantitatively analysed using XRD, TG, and FTIR, and the changes in hydration process were clarified. These results provide a theoretical basis for practical engineering applications and the economic benefits of using FA in high-water materials.

2 Materials and methods

2.1 Material

In this study, CSA cement, FA, dihydrate gypsum, and hydrated lime were used as binder materials to prepare high-water materials. The high-water materials consisted of A, AA, B, and BB. Component A consisted of CSA cement and FA, and AA represented compound retarder. Component B is a mixture of dihydrate gypsum and hydrated lime in a ratio of 4:1 [45], and BB represents an early strength agent and suspension agent. The chemical compositions of the binder materials are listed in Table 1. The particle size distributions of the CSA cement and FA are shown in Figure 1. As shown in Figure 1, the average particle size of the FA (d90) was 46.8 µm. The average particle size of CSA (d90) was 87.7 μm, and the specific surface area was 534.8 m²·kg⁻¹. The initial and final setting times of the CSA cement were 17 and 35 min, respectively, and the compressive strength was 45.2 MPa when the hydration time was 3 days. Composite additives for high-water-content materials include retarders, quick-setting agents, suspension agents, and early-strength agents.

To study the effect of FA on the properties of high-water materials, the experiment adopted the method of internal mixing using FA to replace the A component of high-water materials in the same amount with a fixed water-to-solid ratio

Table 1: Chemical composition of materials (%)

Materials	CaO	SiO ₂	Al ₂ O ₃	SO ₃	MgO	Fe ₂ O ₃	Loss
CSA cement	48.03	9.93	29.75	6.65	1.92	1.41	2.31
FA	7.84	53.74	24.83	0.60	2.40	9.32	1.27
Gypsum	46.65	1.80	0.20	47.65	2.57	0.06	1.07
Lime	87.13	1.34	0.75	0.15	8.97	0.13	1.53

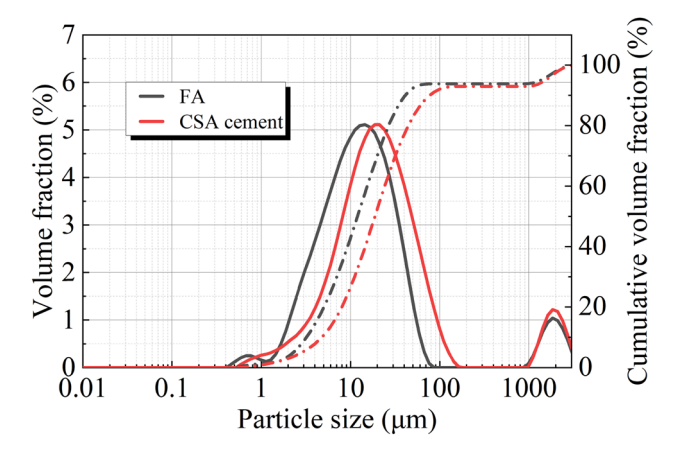


Figure 1: FA and CSA particle size distribution.

of 3.0. The mix proportions of the high-water material are shown in Table 2, and a sample preparation flowchart is shown in Figure 2. The following process was used: The masses of components A, B, and water were weighed according to the specified proportions. The mixture was poured into the two blenders, respectively in the order of adding water first and then adding the powder materials and was stirred for 3 min. Notably, the mixing order was important; first, the group B + BB was mixed, and then group A + AA was mixed. The stirred group A + AA slurry was poured into the mixing pot containing group B + BB slurry and stirred for 5 min to complete the preparation of the high-water slurry system. Finally, the slurry was poured into 70.7 mm × 70.7 mm × 70.7 mm moulds for mechanical properties testing and microscopic test sampling.

2.2 Test methods

2.2.1 Macroscopic performance tests

2.2.1.1 Setting time and bleeding

Workability and setting time of high water materials were tested according to MTT 420-1995 "High Water Filling Materials." As shown in Figure 2, after mixing the two slurries into a mould, a group of samples was collected and poured into a beaker to observe the water secretion of the slurry. Simultaneously, the container was tilted every 1-5 min to observe the fluidity of the paste. The testing time could be reduced, and the tilting angle increased as the fluidity decreased. The setting time was defined when the angle was tilted to 45°, and the slurry lost its fluidity.

The phenomenon of bleeding is mainly used to judge the stability of liquid A in two-liquid high-water materials. The specific operation is as follows. To begin, measure out a specific quantity of slurry and carefully transfer it into a beaker. Add the slurry until it reaches the 400 mL mark. Afterwards, seal the container to prevent water loss and monitor the liquid level every 15 min. Bleeding can be

Table 2: Mix design of high-water materials

Test No.	A (%.wt)		B (%.wt)		Compound additive (%.wt)	
	CSA Cement	FA	Gypsum	Lime	AA	ВВ
1	100	0	80	20	0.1	0.1
2	95	5	80	20	0.1	0.1
3	90	10	80	20	0.1	0.1
4	85	15	80	20	0.1	0.1
5	80	20	80	20	0.1	0.1

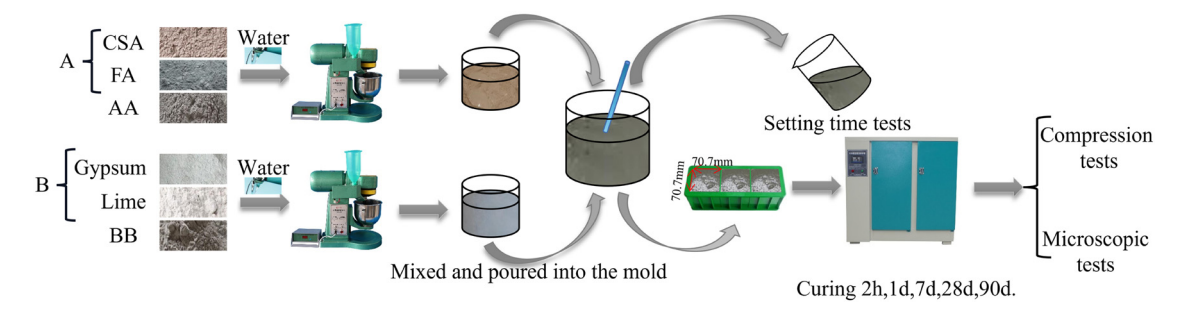


Figure 2: Sample preparation flow chart.

detected when there is a noticeable separation between sediment and clear water.

2.2.1.2 Compressive strength

The compressive strengths of the high-water materials were tested using a TYE-300B pressure testing machine. Three samples for each mixing ratio were tested at the hydration age of 2 h, 1, 7, 28, and 90 days, and the compressive strength was taken as the average of the three samples. The loading speed of the testing machine was controlled in the range of $(1.000 \pm 50) \text{ N·s}^{-1}$.

2.2.2 Microstructure tests

To further explore the influence of FA on the properties of high-water materials, specific samples for microscopic testing were selected based on the macroscopic test data. From the central region of the bulk sample, a cubic sample with a side length of approximately 6-15 mm was selected. Absolute ethanol was used as the displacement solution to terminate sample hydration. The samples with terminated hydration were dried in an oven (40°C, 24 h) and ground into powder form (≤45 µm) for XRD, FTIR, and TG tests. XRD was conducted using a Bruker AXS D8 X-ray diffractometer with a copper target and a scanning speed of 5°·min⁻¹. FTIR testing was performed using an SDT Q600 V20.9 Build 20 instrument, and the test range was 400-4,000 cm⁻¹. TG testing was performed using a PE STA8000. The temperature range was set from room temperature to 800°C, and nitrogen gas was used as the testing atmosphere, with a heating rate of 10°C·min⁻¹.

3 Results

3.1 Setting time and bleeding characteristics

The effect of the FA content on the setting time and bleeding characteristics of high-water materials is shown in Figure 3, which shows that the FA content was positively correlated with the setting time and time when bleeding stopped in the material. When the FA content was <10%, there was no notable effect on the setting time. As the FA content increased, the setting time of the high-water materials increased significantly. When the content reached 20%, the setting time exceeded 20 min. The setting time of high-water-content materials is also an indication of their fluidity. The micromorphology of FA presents a spherical glass body with a smooth surface and a ball effect in the material-mixing slurry [46-48], which can disperse agglomerated CSA cement, gypsum, and hydrated lime particles, thereby increasing the fluidity of the slurry. Consequently, the setting time of the material increases. By contrast, FA exerts a microaggregate effect, better filling the pores between the materials. Because of the small particle size of FA, its lubrication effect can be enhanced [49,50]. However, the binder accounted for only one-quarter of the high-water materials, and this effect was not significant when the fly ash content was relatively low.

Because high-water materials are commonly used for underground filling with a high water-to-solid ratio, the occurrence of bleeding in the filling area could adversely

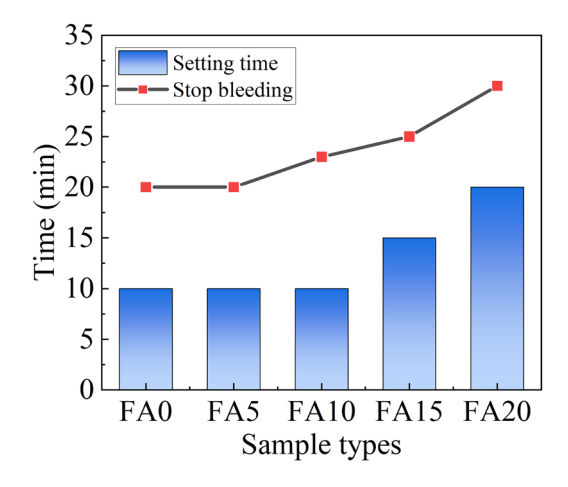


Figure 3: Effect of FA on the setting time and bleeding characteristics.

affect the filling effectiveness. Therefore, it is necessary to control the bleeding of high-water-content materials to ensure that slurries A and B fully react and form a compacted and solidified filling body. The effects of the FA content on the termination time of bleeding and the setting time of the material were similar. When the FA content was <10%, the results were like those in the FA0 group. As shown in Figure 4, the group with an FA content not exceeding 20% had less bleeding, which is prone to reacting with materials and is easily absorbed. This indicates that high-water materials exhibit good water-retaining capacity at this point. Shrinkage was not observed in groups with no more than 15% FA content.

3.2 Compressive strength

The effect of FA content on the compressive strength of high-water materials is shown in Figure 5. The results showed that the FA content significantly influenced the compressive strength development of the high-water materials. When FA was added to the high-water materials, the strength at 2 h and 1 day of hydration was lower than that of the control group, and it gradually decreased with an increase in FA content. Although the strength of the modified high water materials containing FA with a hydration time of 2 h decreased significantly, the strength of the FA5 group with a hydration time of 1 day was only 8% lower than that of the control group. When the hydration time reaches 7 days, the compressive-strength trend of the highwater materials changes. The compressive strength of the high-water materials with 5% FA content was higher than that of the control group, whereas the high-water materials with 10% FA content demonstrated a compressive strength

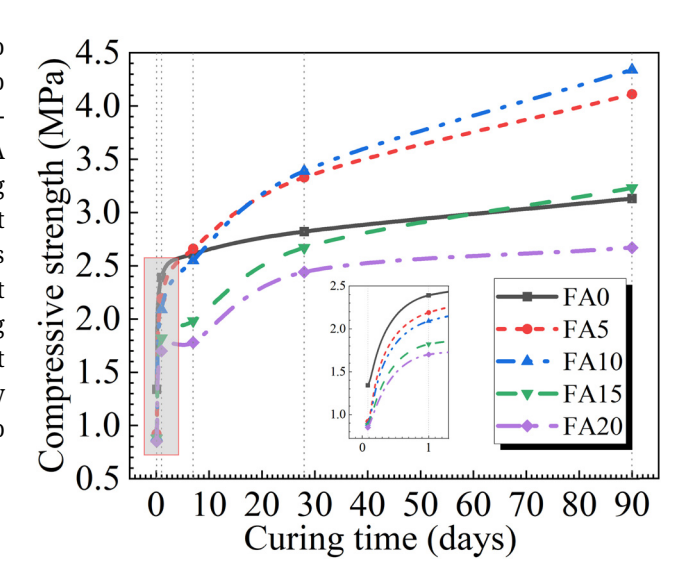


Figure 5: Effect of FA on the compressive strength.

equivalent to that of the control group. The compressive strength of the high-water materials became lower than that of the control group as the FA content increased. With an increase in hydration time, the compressive strengths of the FA5 and FA10 groups increased significantly, and the compressive strength of the FA10 group exceeded that of the FA5 group. Compared to the control group, the compressive strengths of the FA5 and FA10 groups increased by 18.1 and 20.2%, respectively, after 28 days of hydration. At day 90, the FA5 and FA10 groups showed an increase of 31.3 and 38.7%, respectively.

Figure 6 shows the fitting results of the compressive strength of the modified high-water materials and hydration time for different FA contents. Combined with the influence of FA content on the compressive strength of high-water materials, predictive Eqs. (9)–(13) based on



Figure 4: Bleeding characteristics of modified high-water material: (a) FA15, (b) FA20.

6 — Meng Gao et al. DE GRUYTER

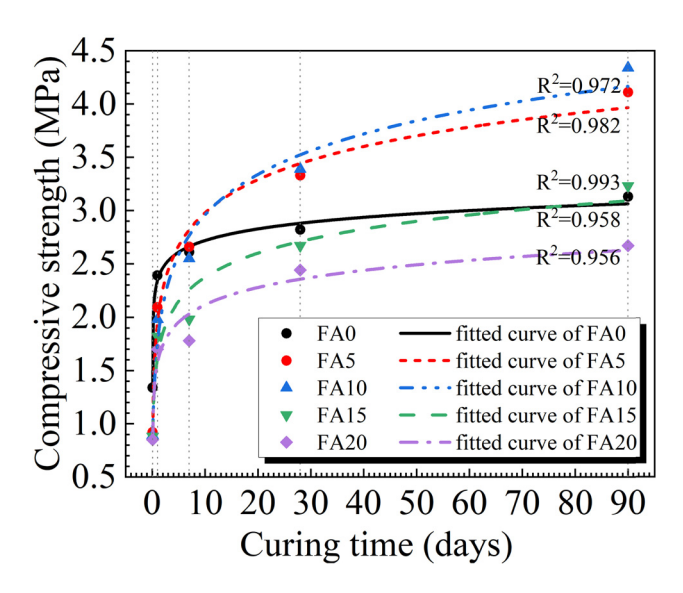


Figure 6: Strength trend fitting curve of high-water materials containing different FA contents.

Eq. (8) were established for the compressive strength of high-water materials with different FA contents.

$$y_a = a - b \cdot \ln(x + c), \tag{8}$$

where y_{α} is the compressive strength of high-water material (α = 0, 5, 10, 15, 20% of FA), x is the curing time of high-water materials (days), and a–c is the regression coefficient.

$$y_0 = 2.359 + 0.156 \cdot \ln(x - 0.082),$$
 (9)

$$y_5 = 2.035 + 0.424 \cdot \ln(x - 0.010),$$
 (10)

$$y_{10} = 1.803 + 0.518 \cdot \ln(x + 0.099),$$
 (11)

$$y_{15} = 1.619 + 0.327 \cdot \ln(x + 0.027),$$
 (12)

$$y_{20} = 1.582 + 0.232 \cdot \ln(x - 0.039).$$
 (13)

When the FA content was 0, 5, 10, 15, and 20%, the R^2 corresponding to the equation were 0.993, 0.982, 0.972, 0.958, and 0.956, respectively. From this, it can be concluded that the curve fitting results are good, indicating that although the strength of the modified high-water material fluctuates, the overall strength of the high-water material shows a logarithmic trend. The regression coefficient, a, in the fitting formula, approximately illustrates the proportion of the initial strength of the high-water material, and the absolute value of b represents the expected rate of strength development of the high-water material in the later stage. Eqs. (9)–(13) shows that the regression coefficient decreases with an increase in the FA content. The -bvalues of the high-water group containing FA were higher than those of the control group, and the maximum value was observed for the high-water group containing 10% FA (-b = 0.518). In summary, the optimal content of FA in

modified high-water materials is 5–10%, which not only has a small loss rate of strength in the early stage of the material but also increases the strength in the later stage. The addition of an appropriate amount of FA to high-water materials is beneficial for ensuring the long-term safety of the filling body.

3.3 XRD analysis

Figure 7 shows the XRD patterns of the hydration products of the modified high-water materials at different hydration ages. Figure 7 shows that the hydration products of the modified high-water materials were mainly composed of ettringite (AFt) and aluminium gel (AH₃). Some non-hydrated SiO₂ and gypsum diffraction peaks were also observed, and strätlingite formed in some modified high-water material groups.

Figure 7(a) and (b) shows the effect of different FA contents on the hydration products of high-water materials at 1 and 28 days hydration time. It can be seen from the figure that AFt is the most abundant hydration product in high-water material systems and the main source of mechanical properties. On the first day of hydration, the AFt peaks of the FA-5 and FA-10 groups were comparable to those of the control group, and the AFt diffraction peaks decreased with increasing FA content. On day 28 of hydration, the AFt peaks were similar in all groups, and the materials containing 10% FA had the highest AFt peaks. Compared to AFt, the diffraction peak of AH₃ was weaker during the entire hydration process of the high-water materials, and no calcium hydroxide (CH) crystals were detected during hydration. This is because CH was consumed by gypsum and FA, and the reaction of gypsum and CH with $C_4A_3\bar{S}$ or AH_3 produces AFt. As the hydration process progressed, the active ingredient in FA underwent a secondary hydration reaction with CH to further consume CH [51]. A new hydration product, strätlingite, was also observed in the high-water material group when the FA content exceeded 10%. Strätlingite is the hydration product of the reaction of C2S in CSA cement with AH3. Weak diffraction peaks of SiO2 and dihydrate gypsum were also observed at diffraction angles of 27.6° and 29.46°, respectively, indicating that the FA, which is a major component of SiO₂, did not fully react with gypsum.

Figure 7(c) shows the XRD patterns of the hydration products of high-water materials containing 10% FA at different hydration times. The peak value of AFt increased significantly with increasing hydration time. This indicates that hydration reactions between the chemical components

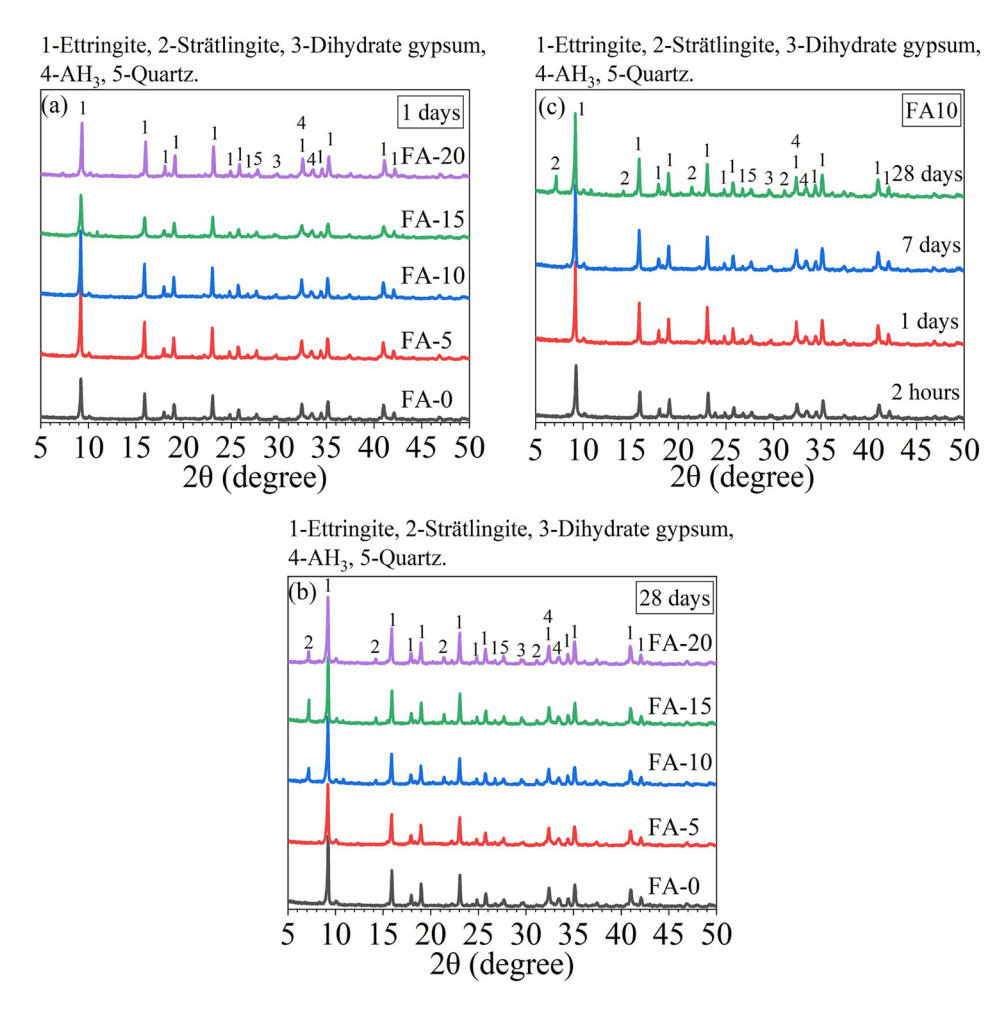


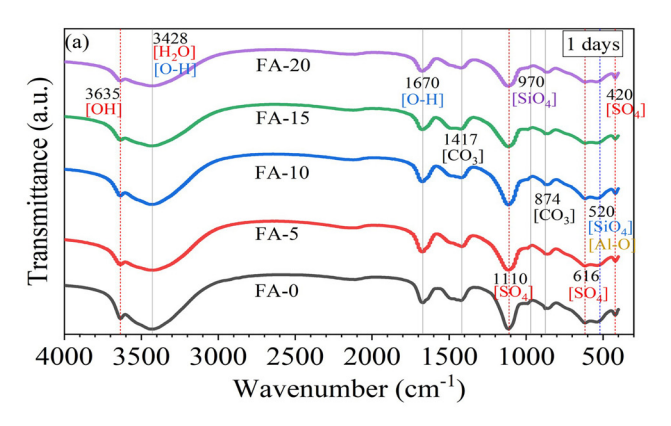
Figure 7: XRD Patterns of modified high-water material under different conditions: (a) curing time of 1 day, (b) curing time of 28 days, and (c) FA content of 10%.

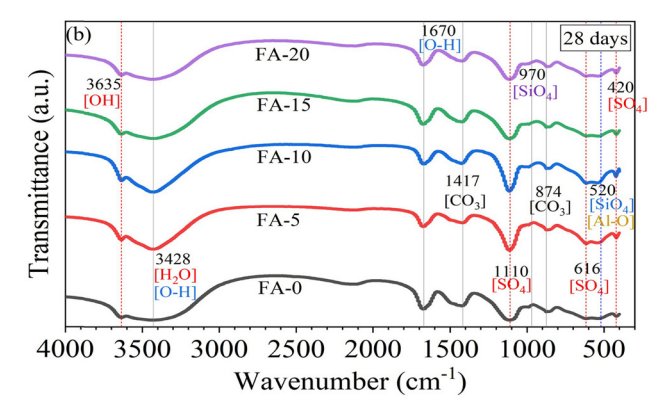
continue to occur as the hydration time increases, resulting in a continuous increase in the strength of the modified high-water materials. Notably, strätlingite appeared in the XRD pattern at 28 days of hydration, whereas no strätlingite was present in the control group (Figure 7(b)). This is related to the FA content of the high-water materials.

3.4 FTIR analysis

FTIR testing was conducted to analyse the changes in the hydration product content of the modified high-water materials at 1 and 28 days of hydration, as well as highwater materials containing 10% FA at different hydration times. The experimental results in Figure 8 show that the hydration products of the hydration process of modified high-water materials were mainly composed of AFt, AH₃, and C-(A)-S-H. Table 3 is the reference table of infrared absorption peaks corresponding to the hydration products of high-water materials [52-54]. By observing the infrared spectra of the hydration products of high-water materials with different FA contents at different hydration ages, ettringite was mainly characterised by the 3,635 cm⁻¹ [OH⁻] absorption band and 1,110 cm⁻¹ [SO₄²⁻] absorption band. Aluminium gel is amorphous, its absorption band is usually flattened and elongated, and the absorption peak at 520 cm⁻¹ is used to characterise aluminium gel. The [SiO₄²⁻] symmetrical contraction vibration occurs at 970 cm⁻¹ and is the main characteristic peak of C-(A)-S-H. The absorption bands at 3,400-3,440 and 1,670 cm⁻¹ are caused by H₂O asymmetric telescopic vibration absorption bands. Although the changes in these absorption bands are more evident, they are also related to the stretching vibrations of structural water in AFt, AH₃, and C-S-H. However, owing to the very close absorption band positions of AFt and monosulphate hydrate (AFm) and the small amount of AFm generated, AFm was not identified in the FTIR spectrum.

8 — Meng Gao et al. DE GRUYTER





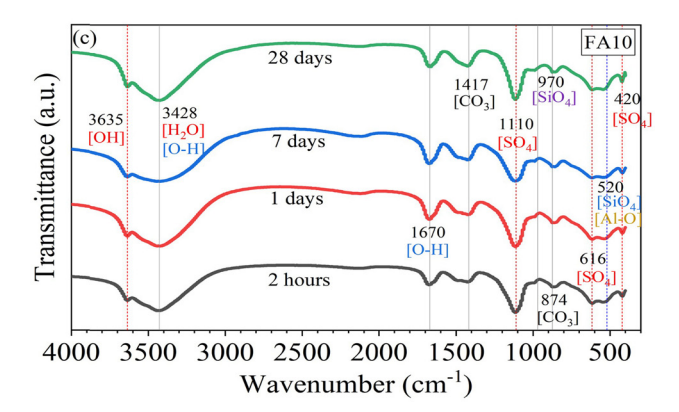


Figure 8: FTIR curves of modified high-water materials under different conditions: (a) curing time of 1 day, (b) curing time of 28 days, and (c) FA content of 10%.

Figure 8(a) shows the effect of FA content on the infrared vibration band of high-water materials at 1 day of hydration. The peak intensities of S–O and H–O bonds in the vibration bands at 1,110 and 3,635 cm⁻¹ gradually decrease with increasing FA content. This indicates that in the early stages of curing, the higher the FA content, the lower the content of the hydration product AFt, with the control group having the highest AFt content. The vibration band at 520 cm⁻¹ also gradually decreases in strength with the increase of FA content. By observing the vibrating band

Table 3: Characteristics of main absorption peaks of FTIR spectrum

	Mode of vibration of functional groups	Wavelength
AFt	[OH] ⁻ stretching vibration	3,635 cm ⁻¹
	[SO ₄] ^{2–} antisymmetric vibration	1,110 cm ⁻¹
	$[SO_4]^{2-}$ bending vibration	616 cm ⁻¹ , 420 cm ⁻¹
AH_3	Al-O	520 cm ⁻¹
	O-H	3,462 cm ⁻¹
C-(A)-S-H	[SiO ₄] ^{2–} Symmetric contraction vibration	970 cm ⁻¹
CaCO ₃	[CO ₃] ²⁻ Vibration of tension	1,417 cm ⁻¹

at 970 cm⁻¹, it can be observed that the Si-O-Si bond strength shows no notable change with increasing FA content. This indicates that the FA content slightly affected the amount of C-S-H gel formed at the initial stage of hydration. Figure 8(b) shows the effect of FA content on the infrared vibration band of high-water materials at 28 days hydration. It can be seen from the figure that the peak intensities of the S-O and H-O bonds in the vibration bands at 1,110 and 3,635 cm⁻¹ increased with increasing FA content and then decreased. The vibrating bands of 5 and 10% FA groups were significantly sharper than those of other groups, and the same changes were observed at 520 cm⁻¹. This indicates that adding 5-10% FA in the later stage of hydration is beneficial for forming AFt and AH₃ in high-water materials. The [SiO₄²⁻] asymmetric telescopic vibration at 970 cm⁻¹ increased with the increase of FA content. The strengths of the absorption bands of the 10, 15, and 20% FA groups showed no noticeable difference, indicating that a limiting value exists for the hydration reaction of FA in high-water materials. The effect of the hydration time on the infrared vibration of high-water materials containing 10% FA is shown in Figure 8(c). The results showed that the peak areas of the vibration bands at 520, 1,110, and 3,635 cm⁻¹ increased as the hydration reaction continued, particularly at 28 days. This indicated that the effect of FA on the hydration characteristics of high-water materials became increasingly evident as the hydration age increased.

3.5 TG analysis

Figure 9(a) and (b) shows the TG and differential thermogravimetric (DTG) curves of the modified high-water materials at 1 and 7 days hydration age. Figure 9(c) shows the TG and DTG comparison curves of the high-water materials with 10% FA modification at different hydration times. Three endothermic peaks appeared in all TG–DTG curves.

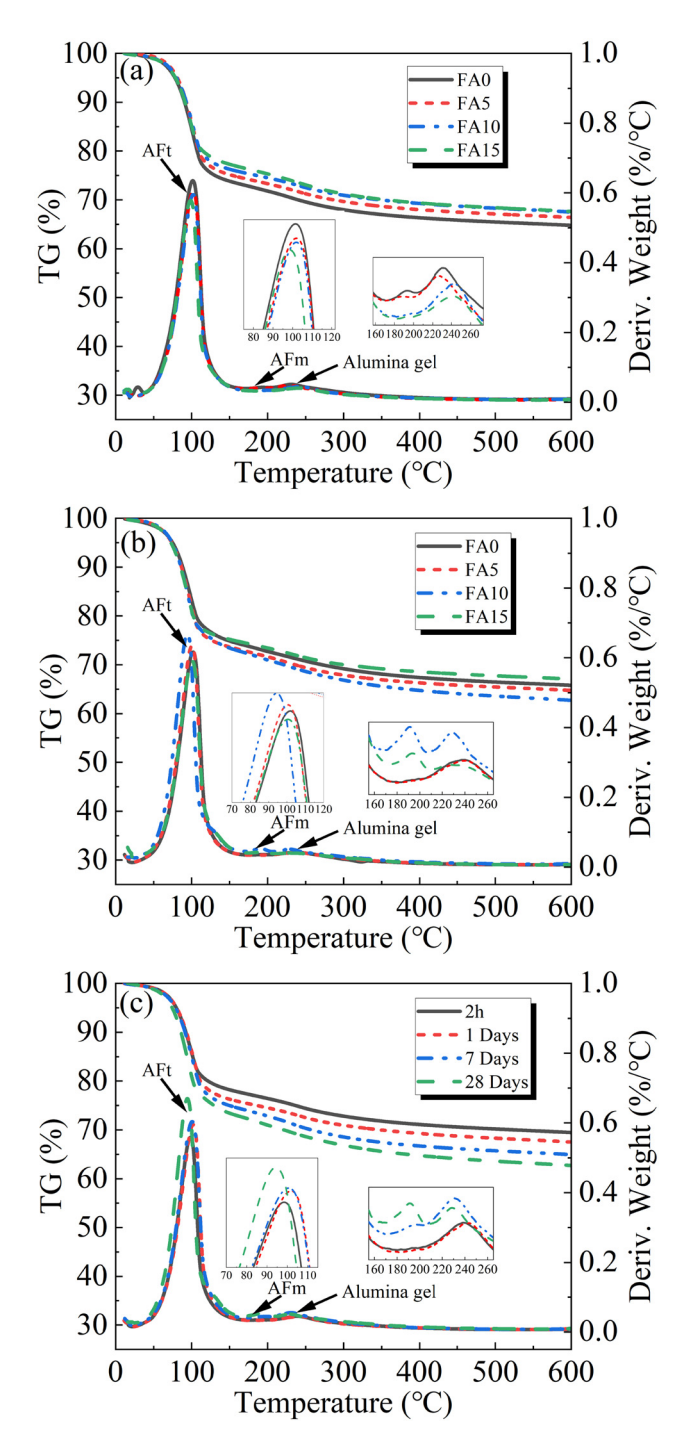


Figure 9: TG-DTG Curves of modified high-water materials under different conditions: (a) curing time of 1 day, (b) curing time of 28 ds, and (c) FA content of 10%.

The first endothermic peak occurred in a temperature range of 50–120°C, and the material mass loss was evident in the TG curve. This temperature range corresponded to the hydrolysis of AFt, which is the main hydration product in high-water materials. The second endothermic peak at ~190°C represents the formation of AFm. The third

endothermic peak at 220–260°C corresponds to the dehydration of AH_3 . The mass loss of the sample during continuous heating corresponding to the ordinate on the left in the figure can be divided into two stages, namely 35–170°C (interlayer free water and AFt bound water detachment) and 170–260°C (AFm and AH_3 dehydration). As shown in Figure 8, the FA content and hydration time of the highwater material samples affected the amounts of AFm, AFt, and AH_3 generated.

Figure 9(a) shows that as the FA content increased from 0 to 15%, the mass loss in Phase 1 decreased from 27 to 23.52%, and the mass loss in Phase 2 decreased from 8.96 to 8.22%. The mass loss was proportional to the corresponding hydration product content at this stage. Therefore, adding FA in the early stages of hydration reduced the amounts of AFt and AH₃ in the high-water materials. When the FA content did not exceed 5%, AFm was generated. There are two main reasons for this. First, the amount of CSA cement decreased owing to the increase in FA content. CSA cement exhibits the characteristics of fast hardening and early strength and is rapidly hydrated in the early stages. FA mainly plays a filling role. Second, the concentration of calcium sulphate in the environment decreases with the hydration reaction, such that the generated AFt is converted to form the AFm phase. Figure 9(b) shows that as the FA content increased, the mass losses in phase 1 were 25.86, 27.16, 27.53, and 25.5%, respectively, and the FA-10 group exhibited the maximum mass loss. The mass losses in phase 2 were 8.34, 8.09, 9.75, and 7.44%, respectively, and AFm generation was performed in all sample sets. Therefore, it can be inferred that the hydration reaction of FA promoted the formation of additional AFt in the system, and gypsum in the system was hydrated to generate AFm at 28 days of hydration. The change in the AH₃ content is related to the FA and C₂S in the system. Figure 9(c) shows that AFt, AFm, and AH₃ were proportional to the heat-absorbing peak area and hydration time. The TG curve shows that with the passage of hydration time, the mass losses in Phase 1 were 22.53, 24.47, 25.89, and 27.16%, and the quality losses of AFt between hydration times were 1.94, 1.42, and 1.27%, respectively. This indicates that although the FA content was only 10%, it also significantly influenced AFt generation.

4 Discussion

The relevant properties of the modified high-water materials were obtained through a series of experiments, and the hydration mechanism of the modified high-water

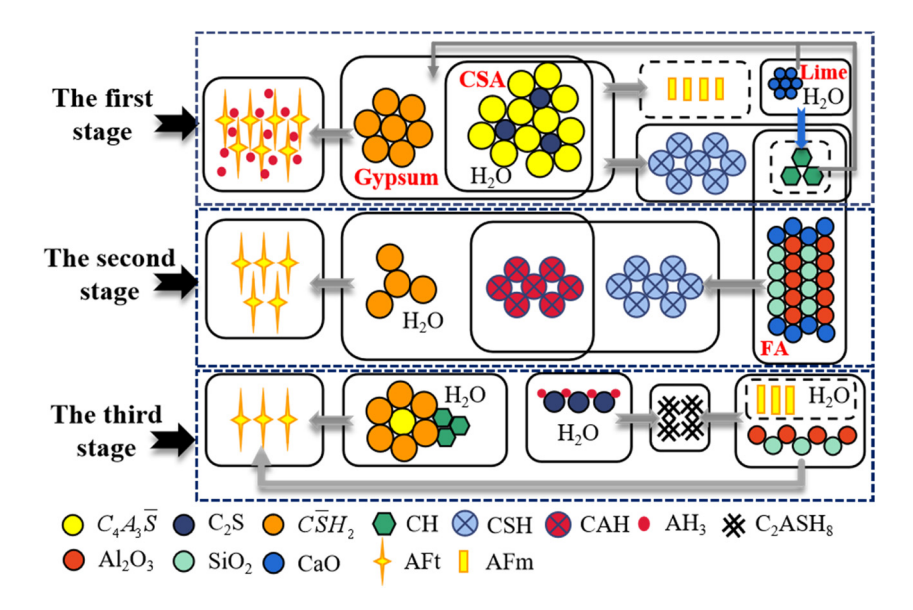


Figure 10: Schematic of reaction process and hydration mechanism of the modified high-water material system.

material system was summarised. The properties of highwater materials were improved by adding FA. The properties of high-water materials depend on their compositions. The main mineral components of CSA cement were $C_4A_3\bar{S}$ and C_2S . The main facies of FA are mullite $(3Al_2O_3\cdot 2SiO_2)$, quartz (SiO_2) , and a small amount of haematite (Fe_2O_3) . The main components of the dihydrate gypsum and hydrated lime were $CaSO_4\cdot 2H_2O$ and CaO, respectively.

When slurries A and B are fused, the $C_4A_3\bar{S}$ in the CSA cement rapidly reacts with the dihydrate gypsum and hydrated lime and generates a large amount of AFt and AH₃ under the action of a coagulant (Eqs. (2), (3), (6), and (7)). Therefore, the XRD, FTIR, and TG results show that AFt and AH₃ were already generated in the samples at 2h of hydration. Al₂O₃ and SiO₂ in FA must be excited in an alkaline environment. The hydration reaction of gypsum, hydrated lime, and C2S in CSA cement can lead to the precipitation of SO_4^{2-} and OH^- , thereby stimulating the FA activity (Eqs. (4), (14), and (15)). FA mainly filled pores in the early stages of hydration. As the hydration process continued, the FA activity began to take effect. Secondary hydration of the FA and CH crystals formed C-S-H and C-A-H gels (Eqs. (16) and (17)), and the C-A-H gel combines with gypsum to produce AFt (Eq. (18)). This explains why the AFt content in FA10 group exceeded that of the control group at 28 days of hydration. Existing studies have shown that the reaction degree of FA in CSA cement systems is only approximately 20% at 90 days [41], indicating that the proportion of the reaction between FA and CH crystals generated by C2S hydration in CSA cement is relatively small. Therefore, the secondary hydration of FA mainly

originates from the CH crystals derived from the hydrated lime, and part of the C₂S reacts with AH₃ to form strätlingite (Eq. (5)). This explains why the TG curve detected a smaller endothermic peak for AH3 at 28 days in the FA10 group compared to the endothermic peak at 7 days. Studies have demonstrated that strätlingite can exist stably in the absence of silicate [55,56]. XRD showed the presence of strätlingite in the samples of high-water materials with FA contents exceeding 10% during later-age hydration. This indicates that when the CSA cement content was less than 90% after 28 days of hydration, the C₂S in the high-water materials group was hydrated. The active ingredients in FA are also related to strätlingite and can produce strätlingite along with AFt (Eq. (19)) [57]. This further confirmed that FA is beneficial for forming AFt in high-water material systems. Finally, the hydration product AFm was not detected by XRD or FTIR. Only a small amount of AFm formation was observed in the TG curve, which was related to the gypsum and FA contents in the system [58]. When the gypsum content in the system was insufficient, the $C_4A_3\bar{S}$ in the CSA cement formed an AFm with water (Eq. (1)). Thus, the amount of AFm generated in the early stage of hydration is proportional to the CSA cement. In the later stage of hydration, the AFm content in the system changed because of the consumption of AFm by the hydration of the active components in the FA (Eq. (19)). After the above analysis, a schematic of the reaction process and hydration mechanism of the modified high-water material was drawn, as shown in Figure 10.

$$CaSO_4 \cdot 2H_2O \rightarrow Ca^{2+} + SO_4^{2-} + 2H_2O,$$
 (14)

$$CaO + H_2O \rightarrow CH$$

$$SiO_2 + n_1Ca(OH)_2 + m_1H_2O$$

 $\rightarrow n_1CaO \cdot SiO_2 \cdot m_1H_2O(CSH),$

$$\begin{split} Al_2O_3 \, + \, n_2Ca(OH)_2 \, + \, m_2H_2O \\ &\rightarrow \, n_2CaO \, \cdot \, Al_2O_3 \, \cdot \, m_2H_2O(C_3AH_6), \end{split}$$

$$C_3AH_6 + 20H + 3C\overline{S}H_2 \rightarrow C_6A\overline{S}_3H_{32},$$
 (18)

$$3C_4A\overline{S}H_{12} + 3S + A + 20H \rightarrow 3C_2ASH_8 + C_6A\overline{S}_3H_{32}$$
. (19)

The contribution of FA content to the main hydration products was analyzed to quantify the mechanical strength of the material. The hydration products that mainly contribute to the strength include AFt, AH₃, C₂ASH₈, and C-S-H. FA reacts with lime to produce C-A-H and C-S-H, and then to produce AFt at the later hydration period (Eqs. (16)–(18)). The gypsum content in the system is insufficient, so CSA cement can be hydrated to produce AFm, and FA can produce AFt and C2ASH8 with it (Eqs. (1) and (19)). The final hydration products obtained from the two hydration reactions significantly contributed more to the strength. In addition, CSA cement content decreases with increasing FA, so the hydration of CSA cement is also analyzed. The hydration of CSA cement is related to gypsum and lime in addition to $C_4A_3\bar{S}$. CSA cement mainly plays the role of early hydration, and the role of FA gradually manifests in late hydration. Therefore, CSA cement consumes gypsum and lime first, and there is an optimal ratio of FA to CSA. The lime did not react completely with CSA cement at the initial stage due to the alkaline liquid phase and the morphological effect of FA. Alkali metal ions attached to the FA surface formed a coating layer, and FA began to hydrate with the extension of hydration time. Second, with the consumption of gypsum, more AFm generated by CSA cement will be converted into more AFt and C₂ASH₈. In summary, gypsum/lime and FA/ CSA cement are closely related. The gypsum/lime in the system is unchanged. Excessive FA content causes a large amount of guick lime to adhere to the FA surface, which corresponds to the low alkalinity provided by CSA cement. The lime hindered a series of hydration reactions of FA (Eqs. (16)-(18)) and CSA cement (Eqs. (6) and (7)), so FA-modified high-water materials have poor early and late strength. The smaller FA content makes the attachment effect of lime weak, and the hydration of CSA cement is dominant, so it has little influence on the early strength. The gypsum content is low in the late hydration stage, and CSA hydration will generate significantly AFm (Eq. (1)). However, low content FA cannot be further transformed with AFm (Eq. (19)), thus restricting the later strength development of high-water materials. Both the strength test and the microscopic results show that the optimum FA content in the high-water system is 10%.

5 Conclusions (15)

(16)

(17)

- This study investigated the influence of FA content on the properties of CSA cement-based materials with high water content, targeting the design of a modified material to improve the setting time and later-age strength. Properties, including setting time, mechanical properties, and hydration evolution, were studied. Based on the obtained results, the following conclusions were drawn:
- a) The influence of the FA content on the setting time of highwater-content materials is limited, particularly when the content is less than 15%. The bleeding cessation time increased with an increase in FA content.
- b) The compressive strength of the high-water materials in the early stages of hydration exhibited a decreasing trend with increasing FA content. The strength after 28 days exceeded that of the control group when the FA content was less than 15%. The modified high-water materials exhibited improved later-age strength.
- Microscopic analysis indicated that AFt and AH₃ were generated at 2h of hydration, which provided early strength to the high-water materials. The FA mainly exhibited a microaggregate effect in the early stages of hydration.
- d) In later-age hydration, FA mainly affects the consumption of gypsum and the C2S hydration process. Strätlingite was detected in the hydration products when the FA content was greater than 10% at 28 days of hydration, further indicating that the incorporation of FA was conducive to the formation of AFt in the CSA cement-based high-water cementitious system, making a greater contribution to the later-age strength.

This study did not analyse the influence of FA on the hydration process of a high-water material system from the perspective of the hydration degree of each component, which has certain limitations. This aspect should be considered in future studies. However, future research on the pore structure will be beneficial for studying the durability of high-water materials.

Acknowledgments: The authors would like to acknowledge the laboratory of the School of Civil Engineering, Henan University of Technology, China, and the staff involved in this experiment.

Funding information: This research was funded by the Key R&D and Promotion Special Program of Henan Province (Research in Science and Technology; No. 222102320092), the Opening Foundation of the Henan Key Laboratory of Grain and Oil Storage Facility & Safety (No. 2022KF08) and

the Innovative Funds Plan of Henan University of Technology (No. 2021ZKCJ17).

Author contributions: Conceptualization, M.G., M.L.; methodology, M.G., M.L.; software, M.L., M.X.; validation and formal analysis, M.L., P.Y.; investigation, J.W., P.Y.; data curation, M.G.; writing - original draft preparation, M.L., M.G.; writing - review and editing, M.G.; visualization, M.X.; supervision, M.G.; project administration, M.G. All authors have accepted responsibility for the entire content of this manuscript and approved its submission.

Conflict of interest: The authors state no conflict of interest.

Data availability statement: All data generated or analysed during this study are included in this published article.

References

- Zhu, C., J. Zhang, M. Li, Z. He, Y. Wang, and Y. Lan. Effect mechanism of strata breakage evolution on stope deformation in extra-thick coal seams. Alexandria Engineering Journal, Vol. 61, No. 6, 2022, pp. 5003-5020.
- Zhou, N., E. Du, M. Li, J. Zhang, and C. Dong. Determination of the [2] stability of residual pillars in a room-and-pillar mining goaf under eccentric load. Energy Reports, Vol. 7, 2021, pp. 9122-9132.
- BP, Statistical review of world energy (2022), 2023. https://www.bp. com/en/global/corporate/energy-economics/statistical-review-ofworld-energy.html.
- Sha, F., C. Lin, Z. Li, and R. Liu. Reinforcement simulation of waterrich and broken rock with Portland cement-based grout. Construction and Building Materials, Vol. 221, 2019, pp. 292-300.
- Zheng, K., D. Xuan, and J. Li. Study on fluid-solid characteristics of grouting filling similar-simulation materials. Minerals, Vol. 12, No. 5, 2022, id. 502.
- Li, P., X. Gao, K. Wang, V. W. Y. Tam, and W. Li. Hydration mechanism and early frost resistance of calcium sulfoaluminate cement concrete. Construction and Building Materials, Vol. 239, 2020, id. 117862.
- Tao, Y., A. V. Rahul, M. K. Mohan, G. De Schutter, and K. Van Tittelboom. Recent progress and technical challenges in using calcium sulfoaluminate (CSA) cement. Cement and Concrete Composites, Vol. 137, 2023, id. 104908.
- Zhang, X., Q. Yang, Q. Li, H. Chen, G. Zheng, and X. Cheng. Effect of phenolic particles on mechanical and thermal conductivity of foamed sulphoaluminate cement-based materials. Materials, Vol. 1221, 2019, id. 3596.
- Li, T., F. Huang, L. Li, J. Zhu, X. Jiang, and Y. Huang. Preparation and properties of sulphoaluminate cement-based foamed concrete with high performance. Construction and Building Materials, Vol. 263, 2020, id. 120945.
- [10] Sha, F., R. Fan, S. Gu, and M. Xi. Strengthening effect of sulphoaluminate cementitious grouting material for water-bearing broken rocky stratum. Construction and Building Materials, Vol. 368, 2023, id. 130390.

- [11] Zhang, J., X. Guan, H. Li, and X. Liu. Performance and hydration study of ultra-fine sulfoaluminate cement-based double liquid grouting material. Construction and Building Materials, Vol. 132, 2017, pp. 262-270.
- [12] Zhou, Y., G. Wang, and Y. Yuan. Basic properties and engineering application of bentonite-cement-water glass grouting. KSCE Journal of Civil Engineering, Vol. 24, 2020, pp. 2742-2750.
- [13] Zhang, Y., S. Wang, B. Zhang, D. Hou, H. Li, L. Li, et al. A preliminary investigation of the properties of potassium magnesium phosphate cement-based grouts mixed with fly ash, water glass and bentonite. Construction and Building Materials, Vol. 237, 2020, id. 117501.
- [14] Wang, A., Z. Li, P. Liu, K. Liu, G. Yu, Q. Zheng, et al. Preparation and Properties of Double Liquid Grouting Materials (DLGMs) Used for the Regenerated Roof of a Coal Mine. Buildings, Vol. 13, No. 3, 2023, id. 584.
- [15] Xu, L., P. Wang, G. Wu, and G. Zhang. Effect of calcium sulfate on the formation of ettringite in calcium aluminate and sulfoaluminate blended systems. Key Engineering Materials, Vol. 599, 2014, pp. 23-28.
- [16] Palou, M. and J. Majling. Effects of sulphate, calcium and aluminum ions upon the hydration of sulphoaluminate belite cement. Journal of Thermal Analysis and Calorimetry, Vol. 46, 1996, pp. 549-556.
- [17] Yu, J., J. Qian, J. Tang, Z. Ji, and Y. Fan. Effect of ettringite seed crystals on the properties of calcium sulphoaluminate cement. Construction and Building Materials, Vol. 207, 2019, pp. 249-257.
- [18] Telesca, A., M. Marroccoli, M. L. Pace, M. Tomasulo, G. L. Valenti, and P. J. M. Monteiro. A hydration study of various calcium sulfoaluminate cements. Cement and Concrete Composites, Vol. 53, 2014, pp. 224-232.
- [19] Yang, J., B. Yang, and M. Yu. Pressure study on pipe transportation associated with cemented coal gangue fly-ash backfill slurry. Applied Sciences, Vol. 9, No. 3, 2019, id. 512.
- [20] Feng, G.-M., H.-C. Chen, T.-M. Chang, and L.-M. Tsai. Early enteral 5% glucose infusion maintains the epidermal growth factor levels in the jejunal flap used for pharyngo-oesophageal reconstruction. Journal of Plastic, Reconstructive & Aesthetic Surgery, Vol. 64, No. 5, 2011, pp. 602-607.
- [21] Liu, J., W. Sui, D. Zhang, and Q. Zhao. Durability of water-affected paste backfill material and its clean use in coal mining. Journal of Cleaner Production, Vol. 250, 2020, id. 119576.
- [22] Xia, J., Q. Su, and D. Liu. Optimal gypsum-lime content of high water material. Materials Letters, Vol. 215, 2018, pp. 284-287.
- [23] Zhang, Y., T. Li, W. Feng, Z. Xiong, and G. Zhang. Effects of temperature on performances and hydration process of sulphoaluminate cement-based dual liquid grouting material and its mechanisms. Journal of Thermal Analysis and Calorimetry, Vol. 139, No. 1, 2019, pp. 47-56.
- [24] Zuo, J., Z. Hong, Z. Xiong, C. Wang, and H. Song. Influence of different W/C on the performances and hydration progress of dual liquid high water backfilling material. Construction and Building Materials, Vol. 190, 2018, pp. 910-917.
- [25] Zheng, Y., W. Xie, Q. Wang, X. Shi, and W. Xie. Effect of silica fume and nano SiO2 on properties of high water materials. IOP Conference Series: Earth and Environmental Science, Vol. 571, No. 1, 2020, id. 012107.
- [26] Zhang, Y., Y. Wang, T. Li, Z. Xiong, and Y. Sun. Effects of lithium carbonate on performances of sulphoaluminate cement-based dual liquid high water material and its mechanisms. Construction and Building Materials, Vol. 161, 2018, pp. 374-380.
- [27] Zhang, L., C. Liu, F. Wu, Y. Lu, and X. Zhou. Study on the characteristics of compressive strength and hydration mechanism of

- high-water-content materials modified by furnace slag and silica fume. IOP Conference Series: Earth and Environmental Science, Vol. 330, No. 4, 2019, id. 042028.
- [28] Wang, J., C. Qian, J. Qu, and J. Guo. Effect of lithium salt and nano nucleating agent on early hydration of cement based materials. Construction and Building Materials, Vol. 174, 2018, pp. 24-29.
- [29] Li, J., R. Wang, and L. Li. Influence of cellulose ethers structure on mechanical strength of calcium sulphoaluminate cement mortar. Construction and Building Materials, Vol. 303, 2021, id. 124514.
- [30] Li, G., J. Zhang, Z. Song, C. Shi, and A. Zhang. Improvement of workability and early strength of calcium sulphoaluminate cement at various temperature by chemical admixtures. Construction and Building Materials, Vol. 160, 2018, pp. 427-439.
- [31] Xiao, R., X. Jiang, Y. Wang, Q. He, and B. Huang. Experimental and thermodynamic study of alkali-activated waste glass and calcium sulfoaluminate cement blends: shrinkage, efflorescence potential, and phase assemblages. Journal of Materials in Civil Engineering, Vol. 33, No. 11, 2021, id. 04021312.
- [32] Xiao, R., B. Huang, H. Zhou, Y. Ma, and X. Jiang. A state-of-the-art review of crushed urban waste glass used in OPC and AAMs (geopolymer): Progress and challenges. Cleaner Materials, Vol. 4, 2022, id. 100083.
- [33] Zhou, Y., Z. Wang, Z. Zhu, Y. Chen, K. Wu, H. Huang, et al. Influence of metakaolin and calcined montmorillonite on the hydration of calcium sulphoaluminate cement. Case Studies in Construction Materials, Vol. 16, 2022, id. e01104.
- [34] Provis, J. L. Alkali-activated materials. Cement and Concrete Research, Vol. 114, 2018, pp. 40-48.
- [35] Zhang, P., C. Wang, F. Wang, and P. Yuan. Influence of sodium silicate to precursor ratio on mechanical properties and durability of the metakaolin/fly ash alkali-activated sustainable mortar using manufactured sand. Reviews on Advanced Materials Science, Vol. 62, No. 1, 2023, id. 20220330.
- [36] Xu, Z., Z. Huang, C. Liu, X. Deng, D. Hui, Y. Deng, et al. Experimental study on mechanical properties and microstructures of steel fiberreinforced fly ash-metakaolin geopolymer-recycled concrete. Reviews on Advanced Materials Science, Vol. 60, No. 1, 2021, pp. 578-590.
- [37] Xiao, R., Z. Shen, R. Si, P. Polaczyk, Y. Li, H. Zhou, et al. Alkaliactivated slag (AAS) and OPC-based composites containing crumb rubber aggregate: Physico-mechanical properties, durability and oxidation of rubber upon NaOH treatment. Journal of Cleaner Production, Vol. 367, 2022, id. 132896.
- [38] Abdulrahman, H., R. Muhamad, P. Visintin, and A. Azim Shukri. Mechanical properties and bond stress-slip behaviour of fly ash geopolymer concrete. Construction and Building Materials, Vol. 327, 2022, id. 126909.
- [39] Qin, L., Z. Xu, Q. Liu, Z. Bai, C. Wang, Q. Luo, et al. Experimental study on mechanical properties of coal gangue base geopolymer recycled aggregate concrete reinforced by steel fiber and nano-Al₂O₃. Reviews on Advanced Materials Science, Vol. 62, No. 1, 2023, id. 20230343.
- [40] Xiao, R., Q. Nie, J. He, H. Lu, Z. Shen, and B. Huang. Utilizing lowlyreactive coal gasification fly ash (CGFA) to stabilize aggregate bases. Journal of Cleaner Production, Vol. 370, 2022, id. 133320.
- [41] Martin, L. H. J., F. Winnefeld, E. Tschopp, C. J. Müller, and B. Lothenbach. Influence of fly ash on the hydration of calcium sulfoaluminate cement. Cement and Concrete Research, Vol. 95, 2017,
- [42] Li, F. Y., L. Chen, G. Q. Li, W. X. Chen, and P. F. Wang. Research on the application of fly ash in high water filling material. Advanced Materials Research, Vol. 807-809, 2013, pp. 1124-1128.

- [43] Feng, B., C. Liu, H. Xie, W. Sun, and Z. Diao. Experimental study and analysis of the mechanical properties of high-water-content materials modified with fly ash. Chinese Journal of Engineering, Vol. 4010, 2018, pp. 1187-1195.
- [44] Sun, D., M. Hu, A. Wang, K. Liu, and Y. Guan. Research and preparation of high water filling material with high dosage of fly ash. Bulletin of the Chinese Ceramic Society, Vol. 35, No. 4, 2016, pp. 1074-1079.
- [45] Shin, G. Y. and F. P. Glasser. Chemistry of cement pore fluids I. Suspension reactions of Ca3-xNa2xAl2O6 solid solutions with and without gypsum additions. Cement and Concrete Research, Vol. 13, No. 3, 1983, pp. 366-376.
- [46] Do, T., H. Kim, K. Minjun, and Y. S. Kim. Utilization of controlled low strength material (CLSM) as a novel grout for geothermal systems: Laboratory and field experiments. Journal of Building Engineering, Vol. 29, 2019, id. 101110.
- [47] Sun, X., H. Liu, Z. H. Tian, Y. Ma, Z. Wang, and H. Fan. Feasibility and economic evaluation of grouting materials containing binary and ternary industrial waste. Construction and Building Materials, Vol. 274, 2021, id. 122021.
- [48] Jin, J., G. Zhang, Z. Qin, T. Liu, J. Shi, and S. Zuo. Viscosity enhancement of self-consolidating cement-tailings grout by biomass fly ash vs. chemical admixtures. Construction and Building Materials, Vol. 340, 2022, id. 127802.
- [49] Garcia-Lodeiro, I., S. Donatello, A. Fernández-Jiménez, and Á. Palomo. Hydration of hybrid alkaline cement containing a very large proportion of fly ash: A descriptive model. Materials, Vol. 9, No. 7, 2016, id. 605.
- Mondal, S. K., C. Clinton, H. Ma, A. Kumar, and M. U. Okoronkwo. [50] Effect of class C and class F fly ash on early-age and mature-age properties of calcium sulfoaluminate cement paste. Sustainability, Vol. 15, No. 3, 2023, id. 2501.
- [51] Trezza, M. A. and A. E. Lavat. Analysis of the system 3CaO·Al2O3-CaSO4·2H2O-CaCO3-H2O by FT-IR spectroscopy. Cement and Concrete Research, Vol. 31, No. 6, 2001, pp. 869-872.
- [52] Toriumi, H. One-and two-dimensional FTIR time-resolved spectroscopy: application to the study of liquid crystal reorientation dynamics. 9th International Conference on Fourier Transform Spectroscopy, Vol. 2089, 1994, pp. 238-239.
- [53] Goudarzi, M., D. Ghanbari, M. Salavati-Niasari, and A. Ahmadi. Synthesis and Characterization of Al(OH)3, Al2O3 Nanoparticles and Polymeric Nanocomposites. Journal of Cluster Science, Vol. 27, No. 1, 2016, pp. 25-38.
- [54] Zhang, W., C. Wei, X. Liu, and Z. Zhang. Effect of phosphorus slag admixture on the properties and hydration mechanism of circulating fluidized bed fly ash-based multi-solid waste cementitious material. Materials, Vol. 1519, 2022, id. 6774.
- Okoronkwo, M. U. and F. P. Glasser. Strätlingite: Compatibility with [55] sulfate and carbonate cement phases. Materials and Structures, Vol. 49, No. 9, 2016, pp. 3569-3577.
- [56] Yuan, Q., Z. Liu, K. Zheng, and C. Ma. Chapter 2 Inorganic cementing materials. In: Civil Engineering Materials, Q. Yuan, Liu, Z., Zheng, K., Ma, C., eds., Elsevier, Netherlands, 2021, pp. 17-57.
- [57] Tang, S. W., H. G. Zhu, Z. J. Li, E. Chen, and H. Y. Shao. Hydration stage identification and phase transformation of calcium sulfoaluminate cement at early age. Construction and Building Materials, Vol. 75, 2015, pp. 11-18.
- Xiao, R., X. Jiang, M. Zhang, P. Polaczyk, and B. Huang. Analytical investigation of phase assemblages of alkali-activated materials in CaO-SiO₂-Al₂O₃ systems: The management of reaction products and designing of precursors. Materials & Design, Vol. 194, 2020, id. 108975.